AIAA AVIATION Forum
August 2-6, 2021, VIRTUAL EVENT
AIAA AVIATION 2021 FORUM

10.2514/6.2021-2543



# Novel Mechanism of Instability Control using Tapered Spike in Hypersonic Flow

Ashish Vashishtha*
*Institute of Technology Carlow, R93 V960, Ireland*

Shashank Khurana†
*BITS Pilani, Dubai, 345055, United Arab Emirates*

**A forward facing spiked blunt nose in high-speed flows is associated with pulsating flow behavior of varying amplitudes depending on spike-nose and length, the forebody geometry and flow conditions. A tapered spike has been proposed as a passive device for reducing these instabilities, which are induced in the flow in place by the straight spikes. Numerical investigation has been carried out using unsteady axisymmetric Navier-Stokes laminar flow solver at hypersonic Mach number 6.0. A flat-tip spike in front of a flat-faced cylindrical forebody, have been simulated for spike length to base diameter ratio, $L/D$ of 0.5, 1.0, 1.5 and 2.0. It has been observed that introduction of taper leads to manipulate the root vortices by elongating it along taper length and reducing the size in transverse direction, which can introduce the stability in the flow field. Additionally, increase in taper angle will lead to reduction in the time-averaged drag coefficient in comparison to the straight spike for all the lengths. The pulsations fluctuations abruptly transition to steady flow with increase in taper (half-cone angle) for all the spike lengths except $L/D$ = 0.5. The required half-cone angle to achieve non-pulsating and stationary flow around spike body reduces with increase in spike length. The corresponding Strouhal number for the flow exhibiting pulsating behaviour was observed higher than 0.1 for the current Mach number and operating conditions.**

## Nomenclature

| | | |
|---|---|---|
| $M_\infty$ | = | Freestream Mach Number |
| $V_\infty$ | = | Freestream Velocity |
| $\rho_\infty$ | = | Freestream Density |
| $P_0$ | = | Stagnation Pressure |
| $P_{ref}$ | = | Reference Pressure (= $\rho_\infty V_\infty^2$) |
| $T_0$ | = | Stagnation Temperature |
| $T_w$ | = | Wall Temperature |
| $L$ | = | Dimensional Length of Spike |
| $d$ | = | Dimensional Diameter of Spike |
| $D$ | = | Dimensional Diameter of forebody |
| $\theta$ | = | Cone half Angle of Tapered Spike |
| $Re$ | = | Reynolds Number |
| $f$ | = | Frequency |
| $St$ | = | Strouhal Number (= $\frac{fL}{V_\infty}$) |
| $C_D$ | = | Drag Coefficient |
| $\sigma$ | = | Standard Deviation |
| $t$ | = | Time |

*Joint First Author, Assistant Lecturer, Department of Aerospace & Mechanical Engineering, IT Carlow, IRELAND, AIAA Member
†Joint First Author, Assistant Professor, Department of Mechanical Engineering, BITS Pilani Dubai Campus, UAE, AIAA Member.

# I. Introduction

A forward-facing spike has largely and unanimously been identified and established as a passive flow control technique to render the strong pressure envelope at the nose in high-speed flows to become weaker. It results in the reduced pressure over the nose, as a consequence of vortices positioned at the spike root, leading to reduction in heat transfer and drag. On the other hand, these key advantages are challenged by the different instabilities brought in the flow with the presence of a protruding spike surface. These high or low frequency instabilities can produce unbalanced normal component of force and cause the flow separation. These uncontrolled fluctuations would produce adverse moments along the surface of the body in consideration, and in some cases could also have a negative effect on the drag reduction. Previous researchers [1–7] have identified different types of unsteadiness in front of various spiked blunt noses in high-speed flows, and analyzed them by using experimental and numerical techniques. Among various studies, Feszty et al. [4–6] has explained the driving mechanism of unsteadiness in front of spiked body as pulsation and oscillation modes in details. Similar pulsations are also observed with other passive controls in hypersonic wind tunnel such as cylindrical arc [8] and hemispherical cavity [9]. Interestingly, the spike which introduces the unsteadiness in unconfined front nose is able to reduce large amplitude fluctuations effectively, when introduced in the hemispherical cavity [10]. Among active control methods, counter-jet flows exhibits the large amplitude fluctuations in large penetration modes, which are similar to spike pulsation mode. Also, the flow-field exhibits small amplitude oscillations in short penetration modes, similar to spike oscillations [11]. Energy deposition methods such as arc discharge [12] and chemical energy [13] have been also subjected to bow-shock fluctuations because of various interactions of flow features.

Understanding the driving mechanism of different instabilities introduced by active or passive methods for drag and heating control is necessary to develop mitigation strategies so that the flow control methods can be effectively utilized in all flow regimes. Khurana and Suzuki [14] extended the studies of aerospikes to lifting-body configurations in Mach 7 flow and proclaimed the presence of a normal force component bringing in instability for the structure. Vashishtha and Khurana [15] investigated the instability for round spike in front of a flat cylindrical forebody at Mach 6 flow. It was observed that the forebody shock of round tipped spike interacts with forebody shock in different manners and consequently results in different pulsation frequencies. The drag coefficient reduces with the increase in spike length, while the amplitude of unsteadiness also increases which brings in significant challenge in the deployment of a spike towards drag control. Vashishtha and Khurana [16] extended the studies of spike instability by introducing a radius of curvature on the previously used flat-faced afterbody [14], and concluded that bringing a curvature reduces the instability and demonstrated stable flow behavior with complete control of pulsation. Focusing on aerodynamic efficiency and reduction in heating, Narayan et al. [17] introduced various geometric modifications on a conventional spike in front of spherical blunt nose, and concluded that stepped tapered spike results in lowest aerodynamic drag and surface heat flux, compared to a straight spike. By taking inference from Narayan et al. [17] study, it is hypothesized that the tapered spike may also contribute to control the pulsations for spiked blunt nose with flat-face forebody. In continuation to the previous studies [15, 16], the effectiveness of the tapered spikes are investigated in this study for drag control as well as pulsation control in flat-faced forebody. A tapered spike is being deemed as a potential technique to beneficially manipulate the forebody shock interaction with spike root. It has been observed that towards the end of collapse phase of shock oscillation, the inflation phase is caused by sharp corner at the flat front phase, which requires a slight build up in pressure for escaping the mass build up in the zone between spike and forebody front face [15]. A small pressure gradient near the corner may reduce the shock unsteadiness, which is believed to be achievable using a tapered spike. In the current study, numerical investigations have been performed with the objective of studying the effect of a tapered spike on flow unsteadiness as well as time-averaged drag, for four different flat nose spike lengths ($L/D$ = 0.5, 1.0, 1.5 and 2.0) with varying cone angles until steady flow is observed.

# II. Numerical Method

In the current study, two-dimensional structured grids have been generated in the computational domain for flat cylindrical base body with straight and tapered spikes. The computations are performed by solving unsteady axi-symmetric Navier-Stokes equations for laminar compressible flows. The spatial inviscid fluxes are evaluated by Lious all-speed AUSM (Advection Upstream Splitting Method) + up scheme [18] with upwind biased third order MUSCL (monotonic upstream-centered scheme for conservative laws) interpolation, while viscous fluxes as well as source terms (because of axisymmetry) are evaluated by using second order central difference scheme. In order to have better accuracy in time domain, the third-order three step TVD Runge - Kutta Method [19] was employed for time integration.

### A. Computational Domain

The computational domain consists of flat-faced cylinder and flat-tip spike. Figure 1a shows overall computation domain with curved inlet, spike, forebody and outlet. Figure 1b shows the two configurations of spikes: straight and tapered spikes. Both the spikes with lengths $L/D = 0.5$, 1.0, 1.5 and 2.0 are simulated. Here, $L$ is the spike length and $D$ is the maximum cross-sectional diameter of the base blunt nose (in current study, $D = 40$ mm). The front face of both straight and tapered spikes are kept as diameter d, where $d/D = 0.1$. The taper angle or half-cone angle of tapered spike is changed in the range of $\theta = 0°$ to 45°, in order to achieve stable flow-field for all the lengths of spikes. Figure 2a and 2b show the structured grid of size $201 \times 121$, generated using elliptic grid generation method for a straight spike geometry and tapered spike geometry, respectively.

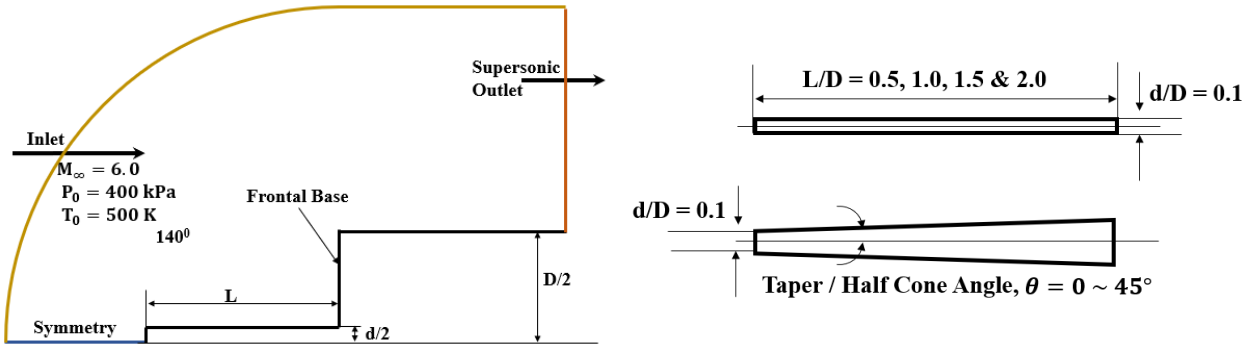


(a) Computational Domain (b) Spike Configurations

**Fig. 1 Geometric Configuration of Spike Body**

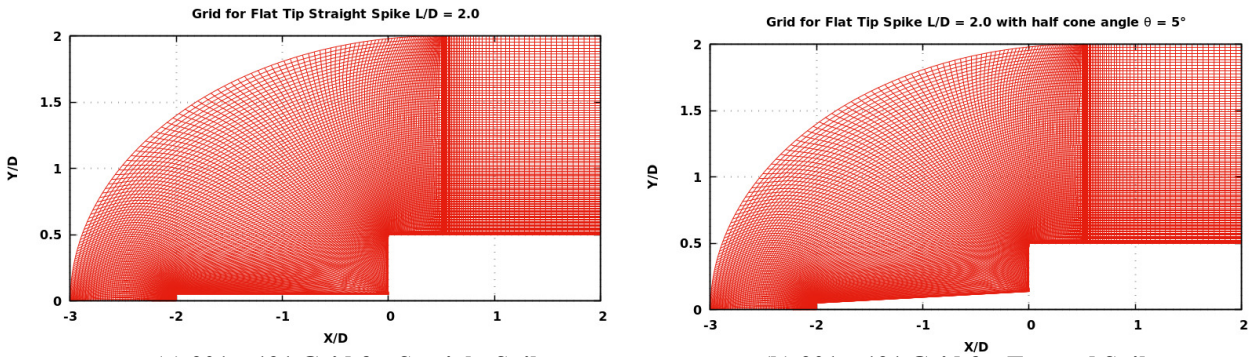


(a) 201 x 121 Grid for Straight Spike (b) 201 x 121 Grid for Tapered Spike

**Fig. 2 Grid used for Straight and Tapered Spikes**

### B. Boundary and Initial Conditions

The inlet boundary condition is used according to VKI Hypersonic Wind Tunnel test-section flow condition, which were used by Feszty [4] at Mach 6.0 hypersonic flow. The stagnation pressure and temperature are considered as 400 kPa and 450 K, respectively. However, the reference length or diameter of blunt nose have been used as 40 mm for current study as shown in Table 1. The Reynolds number based on forebody diameter in the flow-field is 0.134 million. At the wall, no-slip boundary condition along with an isothermal constant wall temperature of 300 K is assumed. The outlet is treated as supersonic outlet with first order interpolation of fluxes from the inner domain. The flow is initiated with hypersonic flow in the domain except around the spike and blunt nose. It is started with low velocity around spike and blunt nose and considered to have an impulse start. All the computations are performed for 4 ms. time duration with physical time step of $1 \times 10^{-9}$s. The same time-step is chosen in order to have CFL number well below 1 for all the computed cases as well as saving time-histories with same time-steps. The results are analysed by computing the drag coefficient at each $1000^{th}$ time-step i.e. at each $1 \times 10^{-6}$s. Further, the frequency of fluctuations are obtained

**Table 1 Inlet Boundary Conditions**

| Property | Specification |
|---|---|
| Mach Number ($M_\infty$) | 6.0 |
| Stagnation Pressure ($P_0$) | 400 kPa |
| Stagnation Temperature ($T_0$) | 450 K |
| Wall Temperature ($T_w$) | 300 K |
| Reference Length ($D$) | 40 mm |
| Reynolds Number ($Re$) | $0.134 \times 10^6$ |

by Fast Fourier Transformation (FFT) of drag coefficient time history and non-dimensional Strouhal Number ($St$) has been computed based on spike length as ($St = \frac{fL}{V_\infty}$), where $f$ is frequency obtained from FFT transformation and $V_\infty$ is freestream velocity.

### C. Grid Independence Study and Code Validation

In order to achieve grid-independent pulsating solution, three different grid sizes coarse ($151 \times 91$), medium ($201 \times 121$) and fine ($261 \times 161$) for straight spike of $L/D = 2$, have been computed with same time-step of $1x10^{-9}$s. The drag coefficient has been computed as well as pressure at $Y = D/4$ location on flat frontal face has been recorded at each 1 $\mu s$. Figure 3a and 3b show the variation of drag coefficient and non-dimensional pressure ($P/P_{ref}$, where

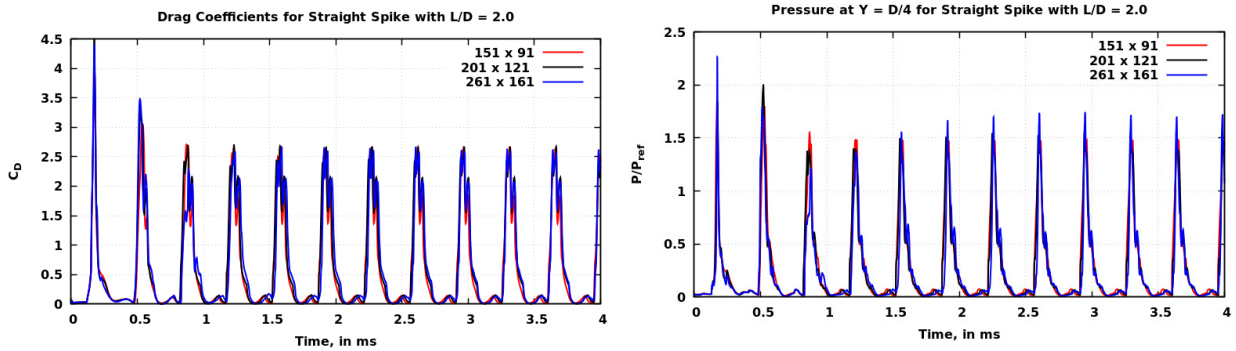


**(a) Drag Coefficient** **(b) Non-dimensional Pressure**

**Fig. 3 (a) Drag Coefficient and (b) Non-dimensional Pressure history for $L/D = 2.0$ straight spike for different grid sizes**

$P_{ref} = \rho_\infty V_\infty^2$) for the total computed time of 4 ms, respectively. The different phases of pulsation fluctuations (as collapse, withhold and inflation) are represented by each cycle in drag coefficient and pressure data. All three grid solutions shows similar trends in both the plots, with minor differences in small fluctuations in initial cycles. Table 2, shows the time-averaged parameters, which are quantifying the pulsation fluctuations. The time-averaged quantities are computed for the duration of 1 ms - 4 ms. The difference in time-averaged drag coefficient is less than 1 % between medium and coarse grid, while the difference in relative standard deviation is approximately 2 %. The time-characteristics, represented by Strouhal Number is same for all three grid sizes. Hence, further medium grid of size $201 \times 121$ has been selected for further computations. The minimum grid size near the wall for the selected grid $201 \times 121$ has been used as $1 \times 10^{-4}$, which represents $4\mu m$ in physical dimension. In order to evaluate the performance of the code, single case from Feszty et al. [4] with 30° conical tipped spike and flat-faced blunt nose in hypersonic flow of Mach number 6, has been simulated. The same case was experimentally studied by Kenworthy [3] among many other configurations of spike and forebody combinations. The simulated case has spike length $L/D = 1.0$ and diameter $d = 0.065D$, where $D = 46$ mm, is the diameter of flat-faced cylindrical blunt nose. Table 3 compares the computed pressure amplitude based on Pressure history at $Y = D/4$ location on flat base as well as Strouhal number (defined as $St = \frac{fD}{V_\infty}$, based on flat blunt nose diameter and freestream flow. The pressure amplitudes are overestimated than comparison to experiments as well as from previous results of Feszty et al. [4]. The peak in pressure time-history is

**Table 2 Time-averaged quantities for spike with $L/D = 2.0$ for various grid sizes**

| Grid Size | Drag Coefficient ($C_D$) | Relative Standard Deviation ($\sigma/C_D$) | Strouhal Number ($St = \frac{f L}{V_\infty}$) |
|---|---|---|---|
| $151 \times 91$ (Coarse) | 0.57167 | 1.332 | 0.2496 |
| $201 \times 121$ (Medium) | 0.63213 | 1.351 | 0.2496 |
| $261 \times 161$ (Fine) | 0.63675 | 1.380 | 0.2496 |

**Table 3 Comparison of time-averaged quantities for Conical Tip Spike with $L = D = 46$ mm, $d/D = 0.065$**

| Property | Experiment Kenworthy [3] | Previous CFD [4] | Current CFD |
|---|---|---|---|
| Pressure Amplitude $\Delta P$ | 1.0378 | 1.6768 | 1.82 |
| Stouhal Number ($St = \frac{f D}{V_\infty}$) | 0.1722 | 0.1800 | 0.1609 |



a sensitive parameter, direct comparison between experiment and CFD should consider cycle to cycle variation, the experimental data acquisition method, pressure transducer area, data reduction methods, pressure sensor mounting method and error in sensor flush mounts etc. Hence, the comparison in pressure amplitude should be considered qualitatively. However, the time characteristics, in terms of Strouhal Number is in good agreement with experiments as well as with previous simulations by Feszty et al. [4]. With the above discussion, it can be concluded that the accuracy of current numerical simulation method is adequate to perform the current comparative study.

## III. Results and Discussions

In the current study, four different flat-tip spikes with lengths $L = 0.5D$, $1.0D$, $1.5D$ and $2.0D$ and diameter $d = 0.1D$ are simulated at hypersonic Mach number 6 by varying the taper angle. The taper angle or half-cone angle ($\theta$) as shown in Figure 1b is varied from 0° for straight spike to maximum 41.97° (case of $L/D = 0.5$ joining corner to spike tip). For the Mach 6.0 free stream conditions (Table 1), the bow-shock is subjected to pulsation mode fluctuations for all the studied $L/D$ ratios of straight spikes. However, it was observed that the increase in taper angle leads to abrupt transition to stable mode from large amplitude pulsation mode for individual spike lengths, except at $L/D = 0.5$. Here, the stable flow means reduction of large amplitude fluctuations and non-stationary flow-field, which leads to almost constant drag force with time variation. For spike with $L/D = 0.5$, it was required to increase taper angle such that it's spike tip corner joins the forebody corner in order to stabilize the flow. On the other hand, for the longest spike with $L/D = 2.0$, a relatively smaller taper angle can bring the stability to the bow-shock and flow-field. Hence the taper angle (or half-cone angle $\theta$) has been varied differently for all four cases. For each spike with different $L/D$ ratio, the results for four to five taper angles are computed. In the following sections, the results are discussed with time-history of drag coefficient plots, Mach contours of cases related to unstable pulsation modes and stable bow-shock formation, comparison of time-averaged quantities as well as time characteristics of pulsations.

### A. Time History of Drag Coefficient

Figure 4 shows the time history of drag coefficient, which was computed at each $1\mu s$ time step for all four spike lengths with various taper angles. At the studied Mach number 6 and wind tunnel test-conditions, flow-field around all the spike lengths exhibit pulsation of large amplitude fluctuations for straight spike. The cycle of pulsation will have three phases as discussed by Feszty et al. [4, 5], collapse, inflation and withhold and the cycle will repeat itself. The collapse is represented in drag curve as increase in the drag coefficient towards the maximum drag, with movement of triple point (of frontal spike bow-shock and forebody shock) towards downstream. The two peaks in drag coefficient represent the movement of triple point near the corner and later the movement of compressed mass from the root of spike in upstream direction as jet, respectively. The inflation, which is triggered by compressed mass at the root of spike and partial mass ejection from the corner leads to decrease in drag coefficient and increase in frontal shock envelop. Near the lowest drag region, there will be momentarily withhold phase until the inflated momentum balances out the upcoming momentum of free-stream flow and formation of triple point occurs. However, the duration of these phases

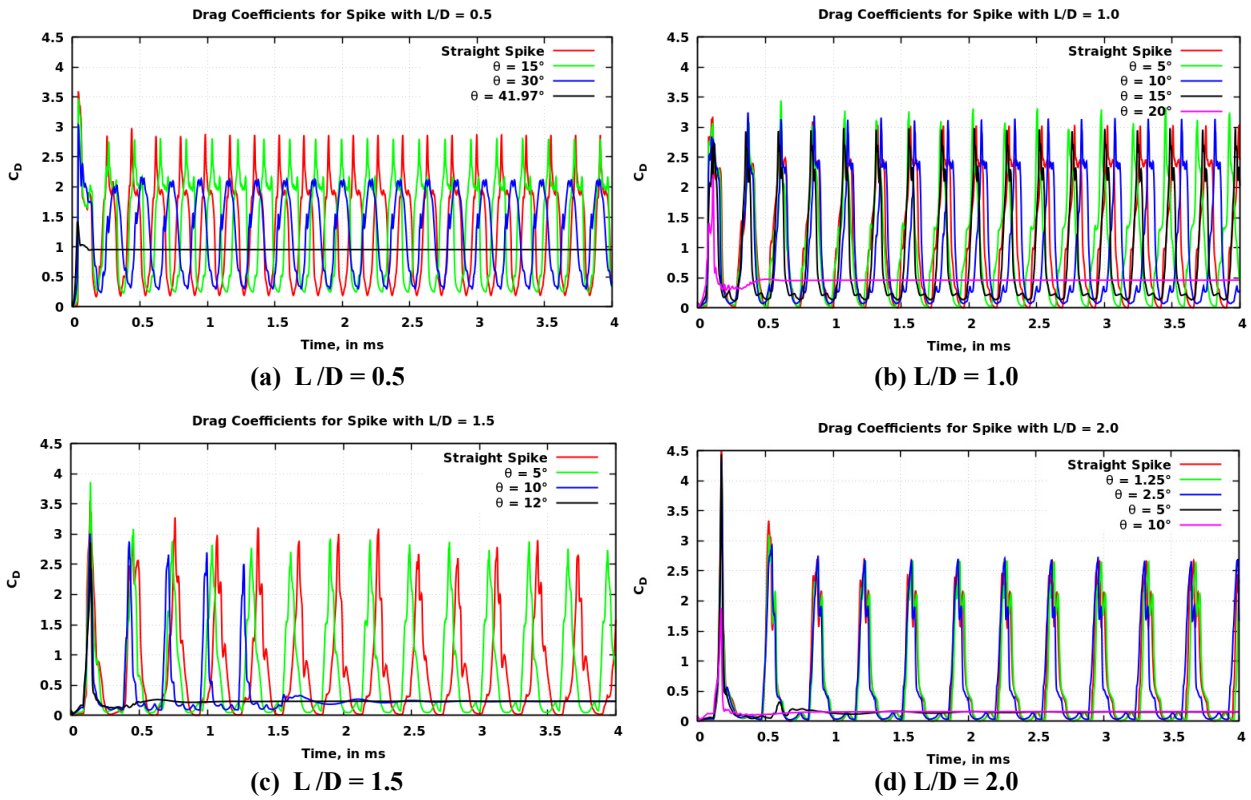


**(a) L /D = 0.5** **(b) L/D = 1.0**

**(c) L /D = 1.5** **(d) L/D = 2.0**

**Fig. 4 Drag Coefficient variation with time for (a) $L/D$ = 0.5, (b) $L/D$ = 1.0, (c) $L/D$ = 1.5 and (d) $L/D$ = 2.0**

will depends on the spike length and diameter of the front face [16]. The smaller spike has the shorter duration of all three phases and the growth of vortex during inflation may occur in both longitudinal and transverse directions. The drag plots for $L/D = 0.5$ show highest numbers of peaks during the 4 ms time history. The number of peaks will reduce with increase in the length of spike in Fig. 4a to 4d. In case of $L/D = 0.5$, the increase in half-cone angle of tapered spike to 15° does not significantly change the dynamics of bow-shock wave, except a slight reduction in number of peaks and because of delay introduced during inflation phase because the compressed mass has to travel longer upstream distance along hypotenuse. Further, increase in the half-cone angle to 30°, will reduce the peak drag as the amplitude of pulsation decreases here. In this case, the stable flow field was not obtained until the corner of spike tip is joined with corner of frontal face at half-cone angle 41.97°. The flow-field transition occur abruptly to stable bow-shock as there was no frontal region to hold any mass. In Fig. 4b, the drag coefficient variation is shown for spike with $L/D = 1.0$. With increase in taper angle from 0° for straight spike to 15°, there will be less significant variations in duration of pulsation phases, while the peak of drag coefficient will remain almost same. When the half-cone angle increases to 20° at $L/D = 1.0$, there is absence of pulsation motions and bow shock remain stable. At spike length to forebody ratio $L/D = 1.5$, the straight spike ($\theta = 0°$ ) and tapered spike with half-cone angle 5° show the pulsation motion with slight difference in duration of pulsation phases. Interestingly, at half-cone angle 10° for $L/D = 1.5$, there are five pulsation cycles observed, which turns into damped oscillations, abruptly between $t = 1.5$ ms to 2.5 ms and the drag coefficient becomes completely stable after $t = 2.5$ ms. In case of spike with $L/D = 2.0$, the minor change in half-cone angle $\theta = 5°$, will lead to stable flow-field. However, there are insignificantly small amplitude oscillations are observed for $\theta = 5°$ up to $t = 2.5$ ms, but for $\theta = 10°$, flow field remains stable after the initial impulse. The above observations suggests that increase in taper angle introduce stability in the pulsation motion of bow-shock by manipulating the root vortex by elongating it along the tapered longitudinal direction and reducing its traverse size. Overall, the aspect ratio of the vortical region changes with introduction of tapered spike and after a certain aspect ratio the mass trapped between the bow-shock, spike and front face may not hold enough momentum to sustain pulsation motion. Hence, there is abrupt change in pulsation to stable drag coefficient.

### B. Pulsation Mode Analysis

In order to understand the vortex manipulation by tapered spike, the Mach contours are analysed for a single cycle of pulsation as well as for the stable configuration of all the lengths of spikes. Figure 5a shows the time-synchronized drag coefficient plot for the straight and various tapered spikes with $L/D = 2.0$ for the duration of 0.4 ms. The drag plots have been plotted for straight spike with $\theta = 0°$, and tapered spikes with half-cone angle $\theta = 1.25°$, $2.5°$ and $5°$. The corresponding Mach contours at various time-steps are also plotted in Fig.5 for $\theta = 2.5°$ to discuss the different phases in pulsation mode. Different phases (inflation, collapse and withheld) of pulsation cycle can be observed in Fig. 5a for $\theta = 0.0°$, $1.25°$ and $2.5°$. At $\theta = 5.0°$, the drag coefficient will remain constant as shown in straight line. For the straight spike and the lower taper angle spikes, the drag coefficient shows initial small peak near to zero drag coefficient before sudden jump in drag coefficient, which triggers the collapse phase. Further, three peaks of higher drag coefficients are observed for $\theta \leq 1.25°$ during pulsation phase. These three peaks represent 1) the movement of triple point towards the flat-face of forebody which leads to increase in high pressure at the front face, 2) movement of triple point (spike shock and forebody shock interaction pint) in transverse direction and passing from corner, which results in relaxation by mass escape and 3) ejection of jet in upstream direction by compressed fluid at spike root. After these three-peaks, the inflation is observed when the drag coefficient suddenly drops to lower values, and the pulsation cycle continues in similar manner. Although straight spike and small taper spike of $\theta = 1.25°$ shows similar trends in the drag coefficient, the taper spike with $\theta = 2.5°$ show slight delay in collapse progression phase and only two significant high drag coefficient peaks, the smaller transverse flat-face of forebody will leads to smaller movement of triple point in transverse direction and mass escape from corner is facilitated. Figure 5b shows the Mach contours at time $t = 2.75$ ms, which represents the inflation phase the lowest drag region, where the frontal bow-shock envelop expands and the triple point can be located past the corner. At time, $t = 2.80$, the freestream momentum overcomes the momentum by upstream flow from spike root, a small curved bow shock at spike tip forms and lead to creation of the triple point in the vicinity. As the shock envelop still expands in comparison to previous time-step, there is drop in drag coefficient as shown in Fig. 5a. After maximum shock envelop expansion, the triple point starts moving towards the flat frontal face,

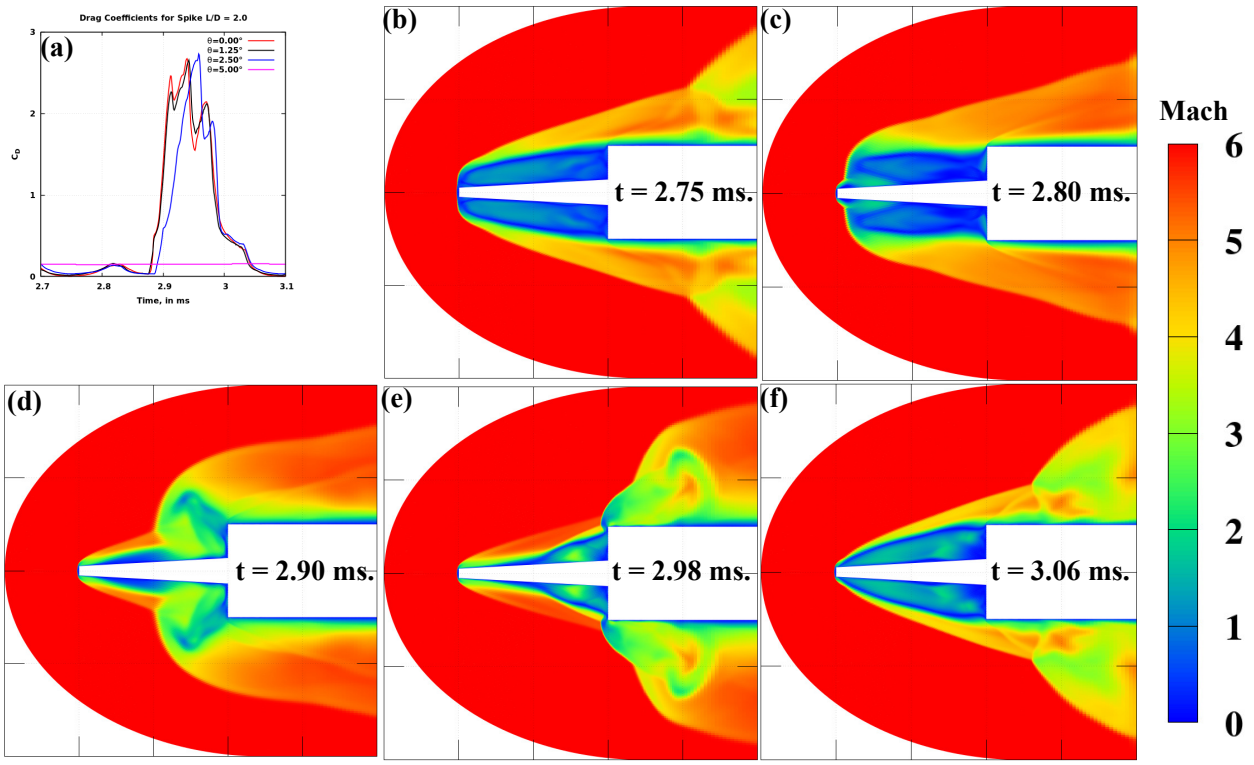


**Fig. 5 (a) Synchronized Drag Coefficient variation in a single cycle for $L/D = 2.0$, with various half-cone angles, and Mach Contours for half-cone angle $\theta = 2.5$ at Time, t = (b) 2.75 ms, (c) 2.80 ms, (d) 2.90 ms, (e) 2.98 ms, and (f) 3.06 ms.**

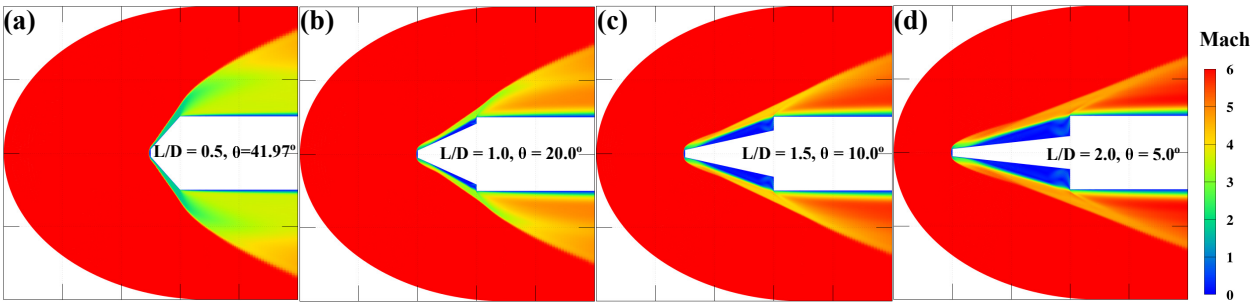


**Fig. 6 Minimum half-cone angles observed for tapered spike with stable flow-field, for $L/D$ = (a) 0.5, (b) 1.0, (c) 1.5 and (d) = 2.0.**



which causes sudden increase in the drag coefficient. Figure 5d shows the movement of triple point and escaping of mass at time, $t$ = 2.90 ms. The high pressure region near the spike root forms and the mass escapes from the corner along with triple point movement from corner at time $t$ = 2.98 ms (Fig. 5e). The high pressure region near the spike root will inflate and flow will move upstream with higher momentum. At the same time, the triple point will cross the corner and move downstream, leads to reduction in drag coefficient. At time, $t$ = 3.06 ms in Fig. 5f, the inflation phase of pulsation fluctuation will continue until the start of new cycle. The introduction of higher taper angle, lead to change the inter-phase flow dynamics of pulsation mode, which can introduce stability. Figure 6 show the Mach contours for minimum half-cone angles simulated in current study with stable (non-pulsating), stationary flow field for spikes with $L/D$ = 0.5, 1.0, 1.5 and 2.0. As discussed with drag coefficient plots, the observed half-cone angle for stable and stationary flow field decreases with increase in $L/D$ ratio. However, in case of $L/D$ = 0.5 the non-pulsating flow is obtained only when the taper is obtained by joining spike tip corner to forebody corner. In this case, the standing bow shock forms at conical section with expansion fans at the corner with stable (free from large amplitude fluctuations) flow-field. In case of $L/D$ = 1.0, for the taper angle of $\theta = 20^\circ$ the stable flow-field is obtained. The standing bow shock forms at almost conical section with smaller region available for vortex formation at the spike root. The bow-shock remain stable and away from the corner of forebody. Spike length $L/D$ = 1.5 shows stable flow field for half-cone angle $\theta = 10^\circ$. However, this configuration shows initial pulsation and after 1.5 ms in drag coefficient plots (in Fig. 4c), it remains stable for the rest of the computed time duration. This configuration shows elongated vortex trapped between spike root, front face of forebody and bow shock away from corner. Similar flow features are observed in $L/D$ = 2.0 case with taper angle $\theta = 5^\circ$. However, this configuration has relatively larger transverse distance available for vortices at root, but overall the elongated vortex at spike root may not have sufficient strength to out-balance pressure behind stable bow-shock. From the geometrical parameters, it is observed that the approximate ratio of available transverse ($D - d - Ltan\theta$) and longitudinal direction ($L$) below 0.125-0.137 shows stable flow behaviour in all the analyzed spike lengths at studied flow condition.

### C. Time Dependent Characteristics

This section relatively quantifies the effectiveness of tapered spike for all the $L/D$ ratios at hypersonic Mach number 6. The time-averaged drag coefficient ($C_D$) has been computed from time-history of Drag Coefficient data (in Fig. 4) for the duration of 3 ms, between 1 ms to 4 ms. The drag coefficient of cylindrical blunt nose without spike has also been computed by simulating it. Fig. 7a shows the time-averaged drag coefficients plotted for all the simulated cases with half-cone angle of spike. It can be clearly observed that the longer straight spikes with flat forebody produce the least drag coefficient among other straight spikes, by pushing the bow-shock at far location. It is also interesting to note that by introducing the taper the drag coefficient in general reduces, for individual spike length. However, once the flow-field is stabilized in case of higher taper angles for $L/D$ =1.5 and 2.0, the time-averaged drag coefficient remain almost constant. Figure 7b shows the percentage reduction in time averaged drag coefficient with respect to without spike blunt nose case. As observed in the trends of drag coefficients, maximum 60 % drag reduction is obtained with straight spike of $L/D$ = 2.0 and atleast 20 % drag reduction is obtained for straight spike of $L/D$ = 0.5. The introduction of taper angle in $L/D$ = 2.0, leads to maximum drag reduction up to 91 % for half-cone angle $\theta = 5^\circ$. At $L/D$ = 1.5, the maximum drag reduction up to 80 % and 81 % have been observed at $\theta = 10^\circ$ & $\theta = 12^\circ$, respectively. The drag reduction for $L/D$ = 1.0 increases from 28 % for straight spike to 78% with tapered spike of half-cone angle $\theta = 20^\circ$. The drag reduction for $L/D$ = 0.5 doubles from 21 % for straight spike to conical blunt nose with flat-tip. Hence it can

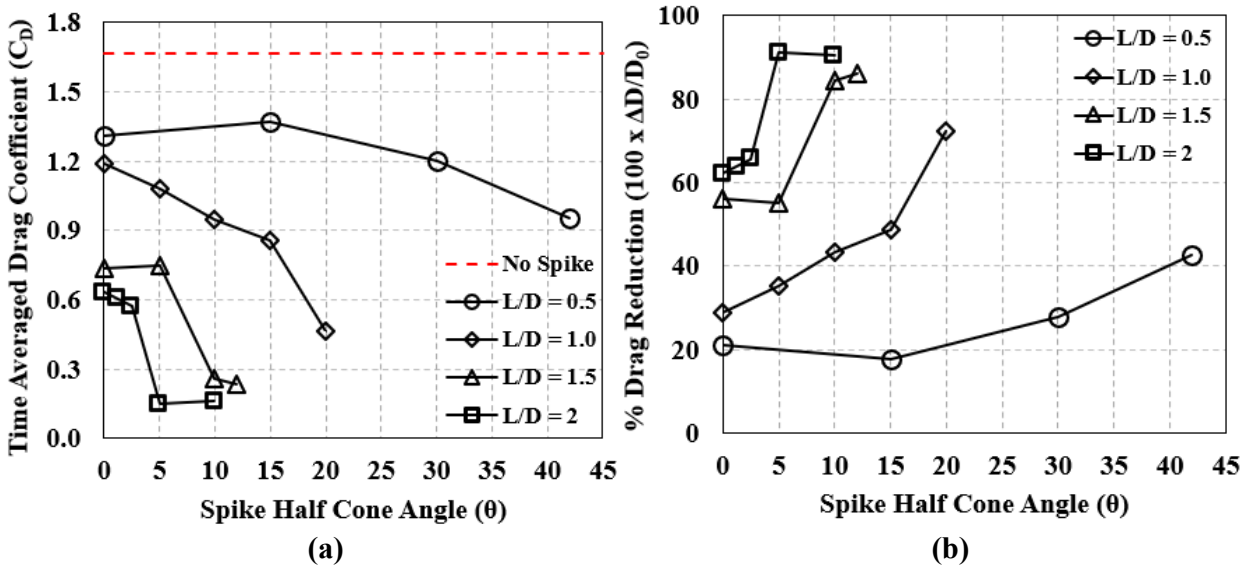


**Fig. 7 (a) Time averaged Drag Coefficient, (b) Reduction in Drag with respect to no spike case.**

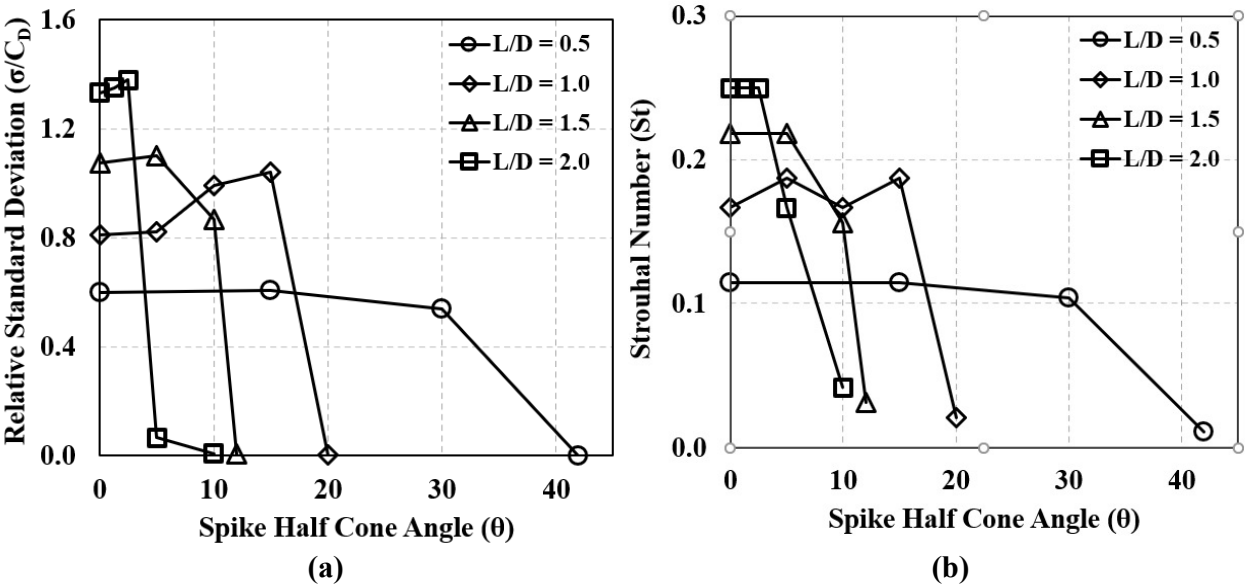


**Fig. 8 (a) Relative Standard Deviations, (b) Computed Strouhal Number based on Spike Length.**

be concluded that tapered spikes can provide stability with appropriate taper angle as well as further reduction in drag coefficient when compared with respective to the straight spike.

To quantify the unsteady characteristics of pulsation mode fluctuations, the relative standard deviation (RSD) plot ($\sigma/C_D$) has been generated for all the spike lengths and taper angles in Fig. 8a. The relative standard deviation can provide an understanding of the variation in amplitude of fluctuations with respect to the mean drag coefficient or drag force. Further, the frequency of fluctuations are computed by Fast Fourier Transformation (FFT) of drag coefficient time-series data from 1ms to 4 ms. The non-dimensional Strouhal number is computed based on spike length and freestream flow velocity as follows:

$$St = \frac{fL}{V_\infty} \tag{1}$$

where, $f$ is the frequency obtained from FFT, $L$ is the spike length and $V_\infty$ is the computed freestream velocity at Mach 6. The Strouhal number is also plotted for all the computed cases in Fig. 8b. The relative standard deviation

remains as high as more that 140 % for $L/D = 2.0$, which abruptly decreases to less than 10 % by introducing the taper angle of 5° and beyond. Similar abrupt changes in relative standard deviations are observed in $L/D = 1.5$, however as $\theta = 10°$ has been observed partially stable (Fig. 4c), hence the plot shows higher relative standard deviation for this particular $\theta$. The higher taper angle, $\theta = 12°$ shows complete reduction in the relative standard deviation, reflects the stable flow-field for the longer duration between 1 ms to 4 ms. In case of $L/D = 1.0$, the relative standard deviation increases with increase in taper angle, until abrupt transition occur to stable flow at $\theta = 20°$. The relative standard deviation remains almost constant for $L/D = 0.5$ and decreases at $\theta = 41.97°$. The correspondingly Strouhal number in Fig. 8b shows similar trends as relative standard deviation. One interesting observation is that the Strouhal number for all the pulsation modes is above 0.1. Although Strouhal number increases with increase in $L/D$ ratio, but the pulsation frequency decreases with increase in $L/D$ ratio, from 5.371 kHz for $L/D = 0.5$ to 2.929 kHz for $L/D = 2.0$. The introduction of taper doesn't change the frequency of pulsation very significantly except in $L/D = 1.5$ & 2.0, at taper angle near stability. Once the flow is stabilized, the Strouhal number suddenly drops below 0.1. It can be concluded from the above discussion that the increase in taper will not change the frequency of pulsation very significantly but, because of interplay between the phases of pulsation, sudden transition to stable flow-field can be obtained.



## IV. Conclusions

The current investigation focused on assessing and controlling the unsteady non-stationary behavior of flowfield in front of spiked flat-faced cylindrical blunt nose with the introduction of a taper at the spike-root. An unsteady two-dimensional axisymmetric Navier-Stokes laminar solver has been utilized for conducting the numerical investigation for spiked blunt nose placed in incoming Mach 6 hypersonic flow. The four spike length ratios $L/D = 0.5$, 1.0, 1.5 and 2.0 are studied for straight as well as tapered spike for various taper or half-cone angles until stationary and stable flow field is obtained at each spike length. It is observed from the drag coefficient time-history that number of pulsation cycles slightly reduce with increase in taper angle and for each spike length, progressive increase in taper angle lead to abrupt transition to stable stationary flow-field. The required taper or half-cone angle decreases with increase in length or $L/D$ ration of spike. The spike with $L/D = 2.0$ will require taper angle $\theta = 5°$ to obtain stable flow field, without any pulsation. However, the required taper angle increases to $\theta = 10°$ for $L/D = 1.5$, $\theta = 20°$ for $L/D = 1.0$ and $\theta = 41.97°$ for $L/D = 0.5$. It is to note that in $L/D = 0.5$ case, require to join spike tip to the corner, which makes a conical blunt nose. The pulsation mode analysis of single cycle suggest that the elongation of vortex region trapped between bow shock, front-face of forebody and spike, can introduce stability in bow shock. It was found that ratio of available frontal transverse direction and longitudinal distance (or spike length) below 0.125 to 0.137 shows stable flow behavior. The analysis of time-averaged drag coefficient suggests that even with long amplitude pulsation, the longer spike $L/D = 2.0$ produced 60 % drag reduction for straight spike, which will increase to 91 % with the introduction of taper angle $\theta = 5°$. At this configuration, the stable flow was also observed. At each spike length ratios $L/D$, the time-averaged drag coefficient reduces with increase in taper angle. The relative standard deviation quantifies the pulsation amplitude, which are more that 140 % of time-averaged drag for $L/D = 2.0$, but it changes abruptly to 10% with introduction of taper angle $\theta = 5°$. The frequency of pulsation does not vary significantly by introducing the taper angle, however, interplay between three phases of pulsation leads to abrupt transition to stable mode. The computed Strouhal number, based on spike length was observed below 0.1 for stable flow-field without any pulsation for all the spike length. Finally, the best performance is observed by $L/D = 2.0$ for overall drag reduction up to 91 % and stationary and stable flow field, which was obtained by introducing small taper angle as $\theta = 5°$.

## References

[1] Maull, D. J., "Hypersonic flow over axially symmetric spiked bodies," *Journal of Fluid Mechanics*, Vol. 8, No. 4, 1960, p. 584–592. https://doi.org/10.1017/S0022112060000815.

[2] Wood, C. J., "Hypersonic flow over spiked cones," *Journal of Fluid Mechanics*, Vol. 12, 1961.

[3] Kenworthy, M. A., "A Study of Unstable Axisymmetric Separation in High Speed Flows," Ph.d. thesis, Virginia Polytechnic Institute and State University, 1978. URL http://hdl.handle.net/10919/76093.

[4] Feszty, D., Richards, B., Badcock, K., and Woodgate, M., "Numerical simulation of a pulsating flow arising over an axisymmetric spiked blunt body at Mach 2.21 and Mach 6.00," *Shock Waves*, Vol. 10, 2000, pp. 323–331. https://doi.org/10.1007/s001930000065.

[5] Feszty, D., Badcock, K. J., and Richards, B. E., "Driving Mechanisms of High-Speed Unsteady Spiked Body Flows, Part I: Pulsation Mode," *AIAA Journal*, Vol. 42, No. 1, 2004, pp. 95–106. https://doi.org/10.2514/1.9034.

[6] Feszty, D., Badcock, K. J., and Richards, B. E., "Driving Mechanism of High-Speed Unsteady Spiked Body Flows, Part 2: Oscillation Mode," *AIAA Journal*, Vol. 42, No. 1, 2004, pp. 107–113. https://doi.org/10.2514/1.9035.

[7] Balakalyani G., J. G., Sriram R., "Shock Tunnel Studies of the Unsteady Hypersonic Flowfield Around Spiked Bodies," *30th International Symposium on Shock Waves 2*, Springer, Cham, 2017, pp. 127–132. https://doi.org/10.1007/978-3-319-44866-4_74.

[8] Vashishtha, A., Watanabe, Y., and Suzuki, K., "Study of Shock Shape in front of Concave, Convex and Flat Arc in Hypersonic Flow," *JAXA Special Publication*, Vol. JAXA-SP-14-010, Japan Aerospace Exploration Agency JAXA, 2015, pp. 127–132. URL http://id.nii.ac.jp/1696/00003852/.

[9] Vashishtha, A., Watanabe, Y., and Suzuki, K., "Study of Bow-Shock Instabilities in front of Hemispherical Shell at Hypersonic Mach Number 7," *45th AIAA Fluid Dynamics Conference*, AIAA 2015-2638, 2015. https://doi.org/10.2514/6.2015-2638.

[10] Vashishtha, A., Watanabe, Y., and Suzuki, K., "Bow-Shock Instability and its Control in front of Hemispherical Concave Shell at Hypersonic Mach Number 7," *Transaction of the JSASS, Aerospace Technology Japan*, Vol. 14, No. ists30, 2016, pp. 121–128. https://doi.org/10.2322/tastj.14.Pe_121.

[11] Jarvinen, P. O., and Adams, R. H., "The effects of retrorockets on the aerodynamic characteristics of conical aeroshell planetary entry vehicles," *8th Aerospace Sciences Meeting*, 1970. https://doi.org/10.2514/6.1970-219.

[12] Erdem, E., Yang, L., and Kontis, K., "Drag Reduction Studies by Steady Energy Deposition at Mach 5," *49th AIAA Aerospace Sciences Meeting including the New Horizons Forum and Aerospace Exposition*, AIAA 2011-1027, 2011. https://doi.org/10.2514/6.2011-1027.

[13] Vashishtha, A., Callaghan, D., and Nolan, C., "Drag Control by Hydrogen Injection in Shocked Stagnation Zone of Blunt Nose," *IOP Conference Series: Materials Science and Engineering*, Vol. 1024, No. 1, 2021, p. 012110. https://doi.org/10.1088/1757-899x/1024/1/012110.

[14] Khurana, S., and Suzuki, K., "Hypersonic Flow Investigation of Aerospikes for Delta type Lifting Body Configurations," *Transaction of The Japan Society for Aeronautical and Space Sciences, Aerospace Technology Japan*, Vol. 10, No. ists28, 2012, pp. Te15 – Te24. https://doi.org/10.2322/tastj.10.Te_15.

[15] Vashishtha, A., and Khurana, S., "On Unsteady Flow Analysis of a Round Spike Blunt Nose Afterbody in Mach 6 Flow," *IOP Conference Series: Materials Science and Engineering*, Vol. 1024, No. 1, 2021, p. 012017. https://doi.org/10.1088/1757-899x/1024/1/012017.

[16] Vashishtha, A., and Khurana, S., "Pulsating Flow Investigation for Spiked Blunt-Nose Body in Hypersonic Flow and its Control," *AIAA Scitech 2021 Forum*, AIAA 2021-0839, 2021. https://doi.org/10.2514/6.2021-0839.

[17] Narayan, A., Narayanan, S., Kumar, R., Singh, T., Kumar, C. S., and Jagadeesh, G., "Control of Aerodynamic Drag and Heating of Nose Cones Through Taper Spikes," *Journal of Spacecraft and Rockets*, Vol. 56, No. 4, 2019, pp. 1165–1176. https://doi.org/10.2514/1.A34250.

[18] Liou, M.-S., "A sequel to AUSM, Part II: AUSM+-up for all speeds," *Journal of Computational Physics*, Vol. 214, No. 1, 2006, pp. 137–170. https://doi.org/10.1016/j.jcp.2005.09.020.

[19] Shu, C.-W., and Osher, S., "Efficient implementation of essentially non-oscillatory shock-capturing schemes," *Journal of Computational Physics*, Vol. 77, No. 2, 1988, pp. 439–471. https://doi.org/10.1016/0021-9991(88)90177-5.